Pomeron cuts and inclusive reactions*

Michael Creutz, Frank E. Paige, and Pu Shen
Brookhaven National Laboratory, Upton, New York 11973
(Received 10 September 1973)

The contributions of Pomeron cuts to inclusive cross sections in the central region are studied within the framework of the Reggeon calculus. The two-particle correlation function contains a term independent of the rapidities of the observed particles and only weakly dependent on the total rapidity Y. The integrated correlation functions f_n grow as Y^{n-1} and satisfy Le Bellac's inequality automatically. The multiplicity distribution contains multiple peaks at very high energy.

I. INTRODUCTION

Since the work of Mueller,[1] the contributions of Regge poles to inclusive cross sections have been studied extensively. If only the poles are considered, then a rather simple picture emerges in which, for example, all correlations have short range in rapidity.[2,3] However, Regge cuts are a natural consequence of unitarity in a theory with Regge poles. Abramovskii, Kanchelli, and Gribov[4] (AKG) have shown recently that within the framework of the Reggeon calculus[5,6] certain Regge cut contributions to inclusive cross sections in the central region can be calculated. After a brief review of their work in Sec. II, this paper is devoted to further examination of these contributions.

In any reasonable energy range the most important correction to the Pomeron pole should come from the graph with one Pomeron loop and no triple-Pomeron vertices. This is because phenomenological estimates of the triple-Pomeron coupling indicate that it is small,[7] while graphs with multiple Pomeron loops are expected to be suppressed. In Sec. III the contribution of this two-Pomeron cut graph to the n-particle inclusive cross section in the central region is studied. The contribution to the single-particle cross section is found to vanish, in accord with the findings of AKG. In fact, if Pomeron interactions are ignored, the leading correction to the single-particle cross section comes from secondary Regge poles, in agreement with Ferbel's analysis.[8] The contribution to the two-particle cross section is best expressed in terms of the two-particle correlation function[2]

$$C(Y,y_1,y_2)=\left(\frac{1}{\sigma}\frac{d\sigma}{dy_1dy_2}\right)\Big/\left(\frac{1}{\sigma^2}\frac{d\sigma}{dy_1}\frac{d\sigma}{dy_2}\right)-1\,, \tag{1.1}$$

where $Y=\ln(s/m^2)$ and y_1 and y_2 are the rapidities of the observed particles. The correlation function is found to be a positive constant independent of y_1 and y_2. Its numerical value in the NAL to CERN-ISR energy range is approximately

$$C(Y,y_1,y_2)\approx\tfrac{1}{2}(\sigma_{\rm diff}/\sigma)\,, \tag{1.2}$$

where $\sigma_{\rm diff}$ is the cross section for diffractive dissociation. The actual Y dependence is more complicated than this. While asymptotically C will behave like Y^{-1}, it is predicted to vary only slowly with Y at presently available energies.

To the constant term in $C(Y,y_1,y_2)$ should be added, of course, the usual short-range term due to secondary Regge poles. The results are then essentially in agreement with the recent conclusions of Botke,[9] whose analysis is based on a qualitative discussion of multiple-exchange effects. Botke also points out that a constant piece in the correlation function would be removed by the choice of a normalization in Eq. (1.1) smaller than the total cross section σ. From a theoretical point of view, it seems preferable to use σ and to recognize that $C(Y,y_1,y_2)$ should contain a constant piece.

Sections IV and V are devoted to a study of the multiplicity distribution. Rules are developed which enable one to write down directly the contribution to the multiplicity-generating function[3] from any Reggeon graph. From the generating function it is simple to obtain the moments of the multiplicity distribution, and the exclusive cross sections σ_n.

In Sec. IV the generating-function method is applied to the pole graph and the two-Pomeron cut graph without triple-Pomeron vertices. The asymptotic form of the integrated correlation function f_n turns out to be

$$f_n\sim[2+(-1)^n](\langle n\rangle)^n\frac{\sigma_{\rm diff}}{\sigma}\,,\quad Y\to\infty$$
$$=O(Y^{n-1})\,, \tag{1.3}$$

where $\sigma_{\rm diff}$, the diffractive cross section, is as-

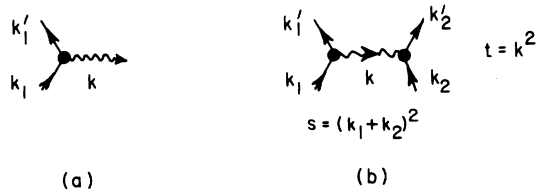

FIG. 1. (a) The basic vertex $\beta(k^2, k_1^2, k_1'^2)$; (b) the Pomeron pole graph.

sumed to be $O(Y^{-1})$, and $\langle n\rangle$ is $O(Y)$. This result is interesting because it automatically satisfies Le Bellac's inequality,[10]

$$\mu_N \equiv \langle (n-\langle n\rangle)^N\rangle \gtrsim (\langle n\rangle)^N \frac{\sigma_{\text{diff}}}{\sigma} \quad \text{for } N \text{ even}. \tag{1.4}$$

By contrast, in a short-range correlation model,[10]

$$\mu_N = O(Y^{N/2}) \quad \text{for } N \text{ even}. \tag{1.5}$$

This is inconsistent with Le Bellac's inequality unless $\sigma_{\text{diff}} \to 0$ faster than any power of Y, implying that the Pomeron has an intercept $\alpha(0) < 1$.

The multiplicity distribution is also obtained in Sec. IV and found to agree with that in Ref. 4. There is a peak at low n corresponding to quasi-elastic scattering, the usual peak at $\langle n\rangle$ with essentially a Poisson distribution, and a third peak at $2\langle n\rangle$, also with essentially a Poisson distribution. At energies in the NAL to CERN-ISR range, these peaks merge to form a distribution that is smooth but wider than a Poisson distribution. Ter-Martirosyan[11] has shown that such a form is consistent with the available data.

In Sec. V the simplest graphs involving triple-Pomeron vertices are considered. While the contributions of these graphs are expected to be small, they are of theoretical interest because they involve the problem of renormalization in the Reggeon calculus.[6] They also provide contributions corresponding to high-mass diffractive dissociation.

Throughout this paper the Pomeron is taken to be a simple, factorizable pole with $\alpha(0) = 1$. The triple-Pomeron vertex must then vanish at $t = 0$, both to prevent an infinite renormalization of the pole there[6] and to satisfy the one-particle kinematic sum rule.[12,13] If this result is combined with the two-particle sum rule and reasonable analytic

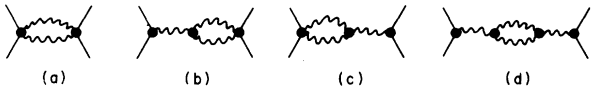

FIG. 2. Pomeron cut graphs for the elastic amplitude.

structure for Reggeon vertices, it leads to the conclusion that the Pomeron must decouple completely at $t = 0$.[13,14] This difficulty is associated only with the requirement of asymptotic self-consistency. It could be cured by modifying the Pomeron at $g_P^2 \ln s \sim 1$, where g_P is a measure of the triple-Pomeron vertex. The difficulty does not manifest itself in any of the calculations in this paper. It therefore seems reasonable to consider the Pomeron to be effectively a simple pole at available energies. All the discussions herein are probably best regarded in this perspective.

II. REGGEON CALCULUS AND DISCONTINUITIES

In this section the Reggeon calculus and the calculation of discontinuities of Reggeon graphs will be reviewed briefly. The only Regge pole considered will be the Pomeron with $\alpha(0) = 1$.

The basic ideas of the Reggeon calculus are abstracted from graphs containing a Pomeron pole $\alpha(k^2)$ coupled with a residue $\beta(k^2, k_1^2, k_1'^2)$ to an elementary particle.[5] See Fig. 1. This pole gives a contribution to the elastic amplitude of

$$F_{\text{pole}}(s, k^2) = \beta^2(k^2)\xi(k^2)(s/m^2)^{\alpha(k^2)}, \tag{2.1}$$

where m^2 is the particle mass, $\beta(k^2)$ is the usual Regge residue,

$$\beta(k^2) = \beta(k^2, m^2, m^2), \tag{2.2}$$

and $\xi(k^2)$ is the signature factor,

$$\xi(k^2) = -\frac{e^{-i\pi\alpha(k^2)/2}}{\sin[\pi\alpha(k^2)/2]}. \tag{2.3}$$

It is assumed that $\beta(k^2, k_1^2, k_1'^2)$ decreases rapidly as any of its arguments become large and that it has only right-hand cuts in these arguments. Within this framework the graphs in Fig. 2 can be calculated.[5,6,15] They give a polynomial in $Y = \ln(s/m^2)$, which polynomial is interpreted as a renormalization of the pole contribution, and a Pomeron-cut term

$$F_{\text{cut}}(s, k_\perp^2) = \frac{i}{4}\int \frac{d^2q}{(2\pi)^2}\,\xi((\tfrac{1}{2}k_\perp + q_\perp)^2)\xi((\tfrac{1}{2}k_\perp - q_\perp)^2)\left(\frac{s}{m^2}\right)^{\alpha((k_\perp/2+q_\perp)^2)+\alpha((k_\perp/2-q_\perp)^2)-1}$$
$$\times\left[\bar{N}(k_\perp, q_\perp) - \frac{g(k_\perp, q_\perp)\beta(k_\perp^2)}{1+\alpha(k_\perp^2)-\alpha((\tfrac{1}{2}k_\perp+q_\perp)^2)-\alpha((\tfrac{1}{2}k_\perp-q_\perp)^2)}\right]^2. \tag{2.4}$$

Here $\bar{N}(k_\perp, p_\perp)$ is the non-Pomeron contribution to the fixed-pole residue in the Pomeron-particle amplitude

$A(s', k_\perp, q_\perp)$ (see Fig. 3),

$$\bar{N}(k_\perp, q_\perp) = \frac{1}{\pi}\int_0^\infty ds' \left[\mathrm{Im}A(s', k_\perp, q_\perp) - \beta(k_\perp^2) g(k_\perp, q_\perp) \left(\frac{s'}{m^2}\right)^{\alpha(k_\perp^2)-\alpha((k_\perp/2+q_\perp)^2)-\alpha((k_\perp/2-q_\perp)^2)}\right], \tag{2.5}$$

and $g(k_\perp, q_\perp)$ is the nonforward triple-Pomeron coupling (Fig. 4).

The total cross section can be obtained from the elastic amplitude by using the optical theorem. Including just the pole and cut graphs of Figs. 1(b) and 2, one finds

$$\sigma(s) = \frac{1}{m^2}\beta^2(0) + \frac{1}{4m^2}\int \frac{d^2q_\perp}{(2\pi)^2}\mathrm{Re}[\xi^2(q_\perp^2)]\left(\frac{s}{m^2}\right)^{2\alpha(q_\perp^2)-2} \times \left[\bar{N}(0, q_\perp) - \frac{g(0, q_\perp)\beta(0)}{1+\alpha(0)-2\alpha(q_\perp^2)}\right]^2 . \tag{2.6}$$

Note that

$$\mathrm{Re}[\xi^2(q_\perp^2)] = \frac{\cos\pi\alpha(q_\perp^2)}{\sin^2[\pi\alpha(q_\perp^2)/2]} \approx -1 , \tag{2.7}$$

so that the cut is negative. Furthermore, the pole dominates the cut as $s \to \infty$ only if[5,6]

$$g(0, 0) = 0 , \tag{2.8}$$

as shall be assumed henceforth.

To obtain inclusive cross sections it is necessary to calculate discontinuities of Reggeon graphs. This problem has been studied in detail by AKG, who make two key observations. Their first observation is that if a certain discontinuity of a graph is to be non-negligible, then that discontinuity must cut through each Reggeon either completely or not at all. This can be seen most easily by thinking of a Reggeon as a generalized ladder graph. Then a cut through only part of the ladder would leave a large-mass cluster hanging from a single line, and would therefore be negligible. See Fig. 5. Of course, a cut through an entire Reggeon takes a simple form:

$$\mathrm{disc}\left[\xi(k^2)\left(\frac{s}{m^2}\right)^{\alpha(k^2)}\right] = 2i\left(\frac{s}{m^2}\right)^{\alpha(k^2)} . \tag{2.9}$$

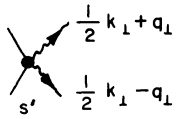

FIG. 3. The Pomeron-particle amplitude.

The second key observation of AKG is that certain Reggeon vertices, including in particular $\bar{N}$ and g, are not changed by cutting. This is true because these vertices are given by integrals with the usual Feynman $i\epsilon$ prescription. On account of the assumed strong damping of the amplitudes, it is always possible to close the contours of the subenergy integrations around the right-hand cuts and thereby effectively to put the intermediate states on the mass shell. A unitarity cut through the graphs also puts the same intermediate states on the mass shell. Therefore, cutting the graph does not change the vertex. For detailed proof see Ref. 4.

To see how the above considerations apply in practice, and also for future reference, it will be useful to review briefly the calculation by AKG of the discontinuity of Fig. 2(a). It is convenient to rewrite the amplitude for this graph from Eq. (2.4) as

$$F(s, k_\perp^2) = -is\int \frac{d^2q_\perp}{4(2\pi)^2} N_{12}^2 (iD_1)(iD_2) , \qquad D_i = \xi(q_i^2)\left(\frac{s}{m^2}\right)^{\alpha(q_i^2)-1} . \tag{2.10}$$

There are contributions to the discontinuity from cuts through zero, one, or two Pomerons. See Fig. 6. The cut through zero Pomerons must pass between the two Pomerons, and either Pomeron can be on either side of the cut. This gives

$$\begin{aligned}\mathrm{disc}_0 F &= is\int \frac{d^2q_\perp}{4(2\pi)^2} N_{12}^2 (D_1 D_2^* + D_1^* D_2) \\ &= +2is\int \frac{d^2q_\perp}{4(2\pi)^2} N_{12}^2 [(\mathrm{Re}D_1)(\mathrm{Re}D_2) + (\mathrm{Im}D_1)(\mathrm{Im}D_2)] .\end{aligned} \tag{2.11}$$

The cut through one Pomeron can pass through either Pomeron, while the other Pomeron can be on either side of the cut. This gives

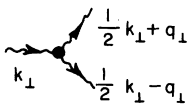

FIG. 4. The triple-Pomeron vertex.

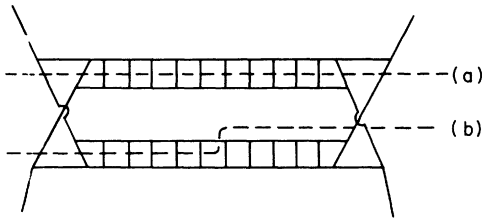

FIG. 5. A ladder graph model. At high energy the cut (a) is non-negligible, while the cut (b) is negligible.

$$\begin{aligned}\mathrm{disc}_1 F &= is\int \frac{d^2q_\perp}{4(2\pi)^2} \\ &\quad\times N_{12}{}^2[(2\,\mathrm{Im}D_1)(iD_2)+(2\,\mathrm{Im}D_1)(iD_2)^* \\ &\quad\quad+(2\,\mathrm{Im}D_2)(iD_1)+(2\,\mathrm{Im}D_2)(iD_1)^*] \\ &= -8\,is\int \frac{d^2q_\perp}{4(2\pi)^2} N_{12}{}^2(\mathrm{Im}D_1)(\mathrm{Im}D_2)\,.\end{aligned} \tag{2.12}$$

Finally, there is only one way to cut through both Pomerons. This gives

$$\begin{aligned}\mathrm{disc}_2 F &= is\int \frac{d^2q_\perp}{4(2\pi)^2} N_{12}{}^2(2\,\mathrm{Im}D_1)(2\,\mathrm{Im}D_2) \\ &= +4is\int \frac{d^2q_\perp}{4(2\pi)^2} N_{12}{}^2(\mathrm{Im}D_1)(\mathrm{Im}D_2)\,.\end{aligned} \tag{2.13}$$

The sum of these three pieces gives

$$\begin{aligned}\mathrm{disc}F &= \mathrm{disc}_0 F+\mathrm{disc}_1 F+\mathrm{disc}_2 F \\ &= 2i\,\mathrm{Im}F\,,\end{aligned} \tag{2.14}$$

as required.

Having found a method for calculating the discontinuities of Reggeon graphs, AKG combined it with Mueller's generalized optical theorem[1,16] to calculate inclusive cross sections in the central region. Their method is as follows. First, a Reggeon graph for the forward elastic amplitude is written as an integral over the transverse momenta $k_{j\perp}$ of the Reggeons and the rapidities ξ_l of any Reggeon vertices. Next, the graph is cut, and for each observed particle with rapidity y_i and transverse momentum $p_{i\perp}$ a vertex $\gamma(p_{i\perp}, k_{j\perp})$ is inserted on a cut Reggeon j whose rapidity span includes y_i. See Fig. 7. This is done in all possible ways. Because of the restriction to the central region, the vertex $\gamma(p_{i\perp}, k_{j\perp})$ does not depend on y_i. At $k_{j\perp}=0$ it is just the usual Mueller vertex.

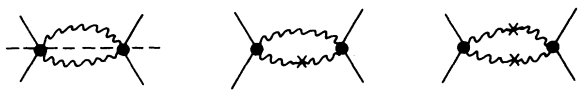

FIG. 6. Graphs for cuts through zero, one, and two Pomerons. A cross denotes a cut Pomeron.

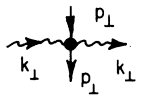

FIG. 7. The vertex $\gamma(p_\perp, k_\perp)$.

Finally, the discontinuity which gives the inclusive cross section,[1,16] $\mathrm{disc}F(s; p_1\cdots p_n)$, is obtained by doing the integrals over the $k_{j\perp}$ and the ξ_l. The limits of the ξ_l integrals will in general introduce dependence on the y_i and Y; any resulting polynomials in these variables are to be interpreted as pole renormalization terms. The inclusive cross section is obtained from

$$\frac{d\sigma}{dp_1\cdots dp_n} = \frac{1}{2is}\mathrm{disc}F(s; p_1\cdots p_n)\,, \tag{2.15}$$

where

$$dp = \frac{d^3p}{(2\pi)^3 2p_0}\,. \tag{2.16}$$

It is also possible that one or more of the observed particles comes from a Pomeron-interaction vertex. This involves new, unknown vertices, but because of the kinematic sum rules these vertices will be of the same order as the triple-Pomeron vertex.[13] If the triple-Pomeron vertex vanishes at $t=0$, then these new vertices will do likewise, implying that the corresponding contributions are of higher order in Y^{-1}. Furthermore, if more than one particle comes from a vertex, then the contribution can be large only when the particles are close together in rapidity.

AKG applied their method to the calculation of a number of contributions to inclusive cross sections. We shall apply the same method in the remainder of this paper. Our calculation differs from theirs mainly in our choice of graphs and in our inclusion of the momentum dependences of the various vertices.

III. UNENHANCED GRAPHS AND INCLUSIVE CROSS SECTIONS

In this section the method developed by AKG and reviewed above will be applied to the unenhanced graphs,[5,6] those with no Pomeron interactions. Particular attention will be given to the effects of the momentum dependence of the vertices. The unenhanced graphs are expected to be important because phenomenological estimates of the triple-Pomeron coupling, while sensitive to the fitting procedure used, indicate that it is small.[7] In particular, its contribution to Eq. (2.6) is much less than that of the vertex $\bar{N}$. Therefore, it is reasonable to make an expansion not only in powers of $(\ln s)^{-1}$, but also in powers of the triple-

Pomeron coupling, or, by extension, in the number of Pomeron-interaction vertices.

In what follows the Pomeron trajectory is taken to be

$$\alpha(k_\perp^2) = 1 + \alpha' k_\perp^2 , \tag{3.1}$$

while the elastic residue function is

$$\beta(k_\perp^2) = \beta_0 e^{\beta_1 k_\perp^2} . \tag{3.2}$$

The fixed-pole residue $\overline{N}$ can be parameterized as

$$\overline{N}(0, q_\perp) = N_0 e^{N_1 q_\perp^2} . \tag{3.3}$$

Then if Pomeron interactions are ignored, Eq. (2.6) for the total cross section takes a simple form:

$$\sigma(s) = \frac{1}{m^2}\left[\beta_0^2 - \frac{N_0^2}{16\pi}\frac{1}{2N_1 + 2\alpha' \ln(s/m^2)}\right] . \tag{3.4}$$

Phenomenological estimates indicate that the eikonal approximation

$$N(0, q_\perp) = \beta^2(q_\perp^2) \tag{3.5}$$

is reasonably good.[15,17] Then $2N_1 + 2\alpha' \ln(s/m^2)$ is just the elastic slope parameter, which for proton-proton scattering is measured to be[18]

$$b(s) = [8.3 + 0.6 \ln(s/m^2)]\,\mathrm{GeV}^{-2} . \tag{3.6}$$

To obtain the correct magnitude for the cut at presently available energies, it is therefore important to retain the constant N_1.

The leading contribution to the n-particle inclusive cross section is just the Pomeron pole graph considered by Mueller.[1] See Fig. 8. It gives an invariant cross section

$$\left.\frac{d\sigma}{dp_1 \cdots dp_n}\right|_{\text{pole}} = \frac{1}{m^2}\beta^2(0)\prod_{i=1}^{n}\gamma(p_{i\perp}, 0) , \tag{3.7}$$

where $\gamma(p_\perp, k_\perp)$ is defined in the previous section and in Fig. 7. In what follows it will be convenient to integrate over the transverse momenta. Therefore, let

$$\gamma(k_\perp^2) = \frac{1}{4\pi}\int \frac{d^2 p_\perp}{(2\pi)^2}\gamma(p_\perp, k_\perp) . \tag{3.8}$$

Then

$$\left.\frac{d\sigma}{dy_1 \cdots dy_n}\right|_{\text{pole}} = \frac{1}{m^2}\beta^2(0)[\gamma(0)]^n , \tag{3.9}$$

where, as usual,

FIG. 8. The pole graph for the n-particle inclusive cross section.

(a) (b)

FIG. 9. The leading cut graphs for the n-particle inclusive cross section. The produced particles in (b) are to be arranged in all 2^n possible ways.

$$p_i = ((p_\perp^2 + m^2)^{1/2}\cosh y_i, p_{i\perp}, (p_\perp^2 + m^2)^{1/2}\sinh y_i) . \tag{3.10}$$

The one-loop graphs without Pomeron interactions are shown in Fig. 9. AKG have shown that the graphs of Fig. 10 with ν exchanged Pomerons give no contribution to the n-particle inclusive cross section for $n < \nu$. Thus Figs. 8 and 9 are the only graphs without Pomeron interactions which contribute for $n \leq 2$. Furthermore, it is evident that graphs involving the exchange of more than two Pomerons are of higher order in $(\ln s)^{-1}$.

From the discussion in Sec. II it is trivial to write down $d\sigma/dy_1 \cdots dy_n$ for Fig. 9. To obtain particles in the central region it is necessary to cut at least one Pomeron. If only one Pomeron is cut, then all of the vertices $\gamma(q_\perp^2)$ must be inserted on that Pomeron. From Eq. (2.12) and (2.15) it follows that this cutting gives

$$\left.\frac{d\sigma}{dy_1 \cdots dy_n}\right|_{\text{Fig. 9(a)}} = -\frac{1}{m^2}\int \frac{d^2 q_\perp}{(2\pi)^2}N^2(0, q_\perp) \times [\gamma(q_\perp^2)]^n \left(\frac{s}{m^2}\right)^{2\alpha(q_\perp^2)-2} . \tag{3.11}$$

Note that this expression is negative, corresponding to absorption of production from a single chain. If both Pomerons are cut, then the vertices $\gamma(q_\perp^2)$ can be divided between the two Pomerons; there are 2^n ways to do this. From Eqs. (2.13) and (2.15) it follows that this cutting gives

$$\left.\frac{d\sigma}{dy_1 \cdots dy_n}\right|_{\text{Fig. 9(b)}} = +2^n\frac{1}{2m^2}\int \frac{d^2 q_\perp}{(2\pi)^2}N^2(0, q_\perp) \times [\gamma(q_\perp^2)]^n \left(\frac{s}{m^2}\right)^{2\alpha(q_\perp^2)-2} . \tag{3.12}$$

Note that this is positive, corresponding to production from two chains. Adding the two contributions gives

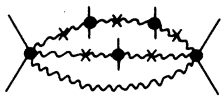

FIG. 10. A nonleading cut graph.

$$\left.\frac{d\sigma}{dy_1\cdots dy_n}\right|_{\text{Figs. 9}} = \frac{1}{2m^2}(2^n-2)\int \frac{d^2q_\perp}{(2\pi)^2}N^2(0,q_\perp)[\gamma(q_\perp^2)]^n\left(\frac{s}{m^2}\right)^{2\alpha(q_\perp^2)-2}, \tag{3.13}$$

which vanishes for $n=1$ in accordance with the general result of AKG mentioned above.

The $k_\perp$ dependence of $\gamma(p_\perp,k_\perp)$ is not directly observable. To estimate this dependence, a simple multi-Regge model is studied in the Appendix. It is found that

$$\gamma(p_\perp k_\perp)\approx \text{const}\times e^{2(\beta_1-\alpha')k_\perp^2}e^{a(p_\perp^2+k_\perp^2)}, \tag{3.14}$$

where β_1 is given by Eq. (3.2). Evidently from Eq. (3.7) with $n=1$ (see Ref. 19)

$$\frac{1}{a}=\langle p_\perp^2\rangle \approx 0.16\ \text{GeV}^2. \tag{3.15}$$

From Eqs. (3.8) and (3.14),

$$\gamma(k_\perp^2)=\gamma_0 e^{\gamma_1 k_\perp^2},\qquad \gamma_1 = a+2(\beta_1-\alpha'). \tag{3.16}$$

The observed values of $\langle p_\perp^2\rangle$ and of the proton-proton elastic slope parameter yield

$$\gamma_1 \approx 10\ \text{GeV}^{-2}. \tag{3.17}$$

It must be recognized that the value of γ_1 is subject to a large theoretical uncertainty.

Using the above form for $\gamma(k_\perp^2)$ enables one to calculate the cut contribution from Eq. (3.13). Adding to it the pole contribution gives

$$\frac{d\sigma}{dy_1\cdots dy_n} = \frac{1}{m^2}\left[\beta_0^2\gamma_0^n+\frac{(2^n-2)N_0^2\gamma_0^n}{8\pi}\frac{1}{2N_1+n\gamma_1+2\alpha' Y}\right]. \tag{3.18}$$

The cut term depends only on $Y=\ln(s/m^2)$, not on $y_1,\ldots,y_n$.

It is customary to define the two-particle correlation function[2]

$$C(Y;y_1,y_2)=\left(\frac{1}{\sigma}\frac{d\sigma}{dy_1dy_2}\right)\Big/\left(\frac{1}{\sigma}\frac{d\sigma}{dy_1}\frac{1}{\sigma}\frac{d}{dy_2}\right)-1. \tag{3.19}$$

From the previous result and Eq. (3.4) for σ,

$$C(Y,y_1,y_2)=\left(1-\frac{N_0^2}{16\pi\beta_0^2}\frac{1}{2N_1+2\alpha' Y}\right)\left(1+\frac{N_0^2}{4\pi\beta_0^2}\frac{1}{2N_1+2\gamma_1+2\alpha' Y}\right)-1$$
$$\approx \frac{N_0^2}{16\pi\beta_0^2}\left(\frac{4}{2N_1+2\gamma_1+2\alpha' Y}-\frac{1}{2N_1+2\alpha' Y}\right). \tag{3.20}$$

Naturally, one must add to Eq. (3.20) the usual short-range correlation due to secondary Regge poles.

Evidently $C(Y,y_1,y_2)$ is independent of y_1 and y_2. Its magnitude and even its sign are dependent on the choice of γ_1. If the above estimate of γ_1 is accepted, and if $2N_1+2\alpha' Y$ is set equal to the elastic slope parameter, Eq. (3.6), then $C(Y,y_1,y_2)$ turns out to be positive and to increase slowly with Y at available energies. Asymptotically it is positive and behaves as Y^{-1}. In the NAL to CERN-ISR energy range its numerical value is given approximately by

$$C(Y;y_1,y_2)\approx \frac{1}{2}\frac{N_0^2}{16\pi\beta_0^2}\frac{1}{2N_1+2\alpha' Y} \approx \frac{1}{2}\frac{\sigma_{\text{diff}}}{\sigma}, \tag{3.21}$$

where the connection between the fixed-pole residue and the diffractive cross section has been used. Thus this calculation is roughly consistent with, although less simple than, the semiquantitative prediction of Botke.[9]

The integrated correlation function is[3]

$$f_2(Y)=\int dy_1dy_2C(Y,y_1,y_2)\frac{1}{\sigma^2}\frac{d\sigma}{dy_1}\frac{d\sigma}{dy_2}. \tag{3.22}$$

Since the correlation function varies slowly with Y, $f_2(Y)$ behaves essentially as Y^2 at available energies.[20] Asymptotically $f_2(Y)$ will grow as Y. Further study of the multiplicity distribution will be deferred to later sections.

In all of the preceding discussion, the transverse momenta $p_{i\perp}$ have been integrated over. The simple multi-Regge model for $\gamma(p_\perp,k_\perp)$, Eq. (3.14), does not couple $p_\perp$ and $k_\perp$, so the $p_{i\perp}$ distributions factorize:

$$\frac{d\sigma}{dp_1\cdots dp_n}=\prod_{i=1}^n\left(16\pi^2 a e^{ap_{i\perp}^2}\right)\frac{d\sigma}{dy_1\cdots dy_n}. \tag{3.23}$$

A more general form for $\gamma(p_\perp,k_\perp)$ could couple $p_\perp$ and $k_\perp$, thereby introducing long-range transverse-momentum correlations. While such corre-

lations would be very interesting, they are obviously model-dependent.

IV. MULTIPLICITY DISTRIBUTIONS AND RELATED TOPICS

The previous section discussed the contributions of the graphs in Fig. 9 to inclusive differential cross sections. This section investigates the multiplicity distribution of the produced particles for the same graphs. We show that the moments of the multiplicity distribution will reflect the long-range correlations introduced by the Pomeron cuts. Furthermore, these correlations are sufficient to satisfy an inequality of Le Bellac.[10] With only short-range correlations this inequality requires the total cross section to decrease faster than any power of $\ln s$.

In order to handle the combinatorial analysis involved in a discussion of multiplicity distributions, it is simplest to use the generating-function technique discussed by Mueller,[3] whose notation we follow. Our formulas can be easily generalized to the generating functional of Shei and Yan[21] and Brown,[22] but this will not be done, in the interest of simplicity.

In terms of the exclusive cross section σ_n to produce n particles and the total cross section σ, the generating function is defined as[3]

$$\psi(\lambda)=\sum_{n=0}^{\infty}\frac{\sigma_n}{\sigma}\lambda^n. \tag{4.1}$$

From $\psi(\lambda)$ we can find the moments of the multiplicity distribution:

$$\begin{aligned}F_N&=\langle n(n-1)\cdots(n-N+1)\rangle\\&=\frac{1}{\sigma}\int dp_1\cdots dp_N\frac{d\sigma}{dp_1\cdots dp_N}\\&=\left(\frac{d}{d\lambda}\right)^N\psi(\lambda)\Big|_{\lambda=1},\end{aligned} \tag{4.2}$$

and

$$F_0=1.$$

The integrated correlation functions are

$$f_N=\left(\frac{d}{d\lambda}\right)^N\ln\psi(\lambda)\Big|_{\lambda=1}. \tag{4.3}$$

The quantities $\psi(\lambda)$, F_N, and f_N all carry an implicit energy dependence.

To calculate $\psi(\lambda)$ we use the relation

$$\psi(\lambda)=\sum_{n=0}^{\infty}\frac{(\lambda-1)^nF_n}{n!}, \tag{4.4}$$

which follows from Eq. (4.2). Using Eq. (3.18) we calculate the contribution to F_n from the graphs of Figs. 8 and 9:

$$m^2\sigma F_n=(\gamma_0Y)^n\left[\beta_0{}^2+\frac{N_0{}^2}{16\pi(2\alpha'Y+2N_1+n\gamma_1)}\times(2^{n+1}-4+\delta_{n0})\right]. \tag{4.5}$$

Substitution of this in Eq. (4.4) gives

$$\begin{aligned}m^2\sigma\psi(\lambda)=\beta_0{}^2e^{\gamma_0Y(\lambda-1)}&+\frac{N_0{}^2}{16\pi\gamma_1}\\&\times\int_0^1\frac{dx}{x}x^{(2\alpha'Y+2N_1)/\gamma_1}\\&\times\left(2e^{2x\gamma_0Y(\lambda-1)}-4e^{x\gamma_0Y(\lambda-1)}+1\right).\end{aligned} \tag{4.6}$$

Equation (3.18) is expected to give correctly only the leading behavior of F_n in Y. There will be additional contributions both from other Pomeron cut graphs and from secondary Regge poles. Thus we should believe only those conclusions derived from Eq. (4.6) which are not affected by such contributions.

The integrated correlation functions f_n are calculated from Eqs. (4.3) and (4.6). We work to leading order in Y and observe that since we are studying $\psi(\lambda)$ for λ near unity, the x integral is dominated by $x\approx 1$. We find for $n\geq 2$

$$f_n=\frac{N_0{}^2\gamma_0{}^nY^{n-1}}{32\pi\alpha'\beta_0{}^2}[2+(-1)^n]+O(Y^{n-2}). \tag{4.7}$$

When $n=2$, we expect additional contributions of $O(Y)$ from short-range effects, so we can only say that the relation $f_2=O(Y)$ is unchanged in the limit $Y\to\infty$ by the cuts being studied in this section. [See, however, the discussion following Eq. (3.22).] For $n=1$ the pole term dominates:

$$f_1=\langle n\rangle=\gamma_0Y+O(1). \tag{4.8}$$

We remind the reader that in a short-range correlation picture one expects all the f_n to grow at most linearly with Y.[2,3] Thus, the Y^{n-1} behavior in Eq. (4.7) reflects the long-range correlations produced by the Pomeron cuts.

It is tempting to calculate the derivatives of $\psi(\lambda)$ at $\lambda=0$ in order to obtain an explicit expression for σ_n. This is a potentially dangerous procedure, as nonleading terms in the F_n will modify the details of the result. In particular, we have not made a definite prediction on f_2, which is closely related to the width of the multiplicity distribution. After calculating the multiplicity distribution in the naive manner, we will comment on which features are most believable.

With this cautionary note in mind we calculate

$$m^2\sigma_n = \frac{1}{n!}\left(\frac{d}{d\lambda}\right)^n [m^2\sigma\psi(\lambda)]\Big|_{\lambda=0}$$

$$= \beta_0{}^2 \frac{(\gamma_0 Y)^n}{n!} e^{-\gamma_0 Y} + \frac{N_0{}^2}{16\pi\gamma_1}\int_0^1 \frac{dx}{x} x^{(2\alpha' Y + 2N_1)/\gamma_1}\left(2\frac{(2x\gamma_0 Y)^n}{n!}e^{-2x\gamma_0 Y} - 4\frac{(x\gamma_0 Y)^n}{n!}e^{-x\gamma_0 Y} + \delta_{n0}\right). \tag{4.9}$$

The first term in this expression is a Poisson distribution centered at $\gamma_0 Y$ coming from the pure pole diagrams. The three terms under the integral correspond to the three possible cuttings of the cut graph, Fig. 6. The first of these terms comes from cutting both Pomerons. This cutting gives a superposition of Poisson distributions weighted with the factor $x^{(2\alpha' Y + 2N_1)/\gamma_1 - 1}$. As Y becomes large, this factor peaks strongly at $x = 1$; consequently, we obtain essentially a Possson distribution peaked at $2\gamma_0 Y$. Similarly the second term is essentially a Poisson distribution centered at $\gamma_0 Y$. The negative sign in front of this term indicates that it acts to reduce the number of particles in the Poisson distribution coming from the pure pole diagram. Finally we come to the interesting δ_{n0} term. Since our model is only valid for produced particles in the central region of rapidity space, a term δ_{n0} should be interpreted as meaning that no particles are present in the central region. In other words, this term represents diffractive dissociation of the initial particles into low-mass hadronic systems. Inclusion of short-range correlation effects will spread this contribution over small values of n. Thus we find the diffractive cross section

$$\sigma_{\text{diff}} = \frac{N_0{}^2}{32\pi\alpha' m^2 (Y + N_1/\alpha')}. \tag{4.10}$$

This result is of course consistent with using the diffractive cross section to calculate N.[17] Because of the neglect in this section of Pomeron interactions, we do not find diffractive excitation into massive states. Such processes will be discussed in the next section.

In a natural fashion this model has given rise both to diffractive events and to large multiplicity ones with $\langle n\rangle = \gamma_0 Y$. In addition, the model predicts a peak in the multiplicity distribution at $n = 2\gamma_0 Y$. The total amount of cross section in this second peak is found from Eq. (4.9) to be precisely $2\sigma_{\text{diff}}$.[4] This peak is a definite prediction of the model, although at nonasymptotic energies the peaks at $n = \gamma_0 Y$ and $n = 2\gamma_0 Y$ will merge to form a widened distribution.[11] In the next section we show explicitly how more complicated graphs in the Reggeon calculus partially fill in the gaps between these peaks.

The three-peak structure found here for the multiplicity distribution will become the multiple-peak structure of AKG when multiple Pomeron exchange is included. We do not expect short-range correlations to change substantially the positions of the various peaks or the cross section included under each one. However, we do expect corrections to the detailed shapes of the individual peaks. In general, they will not be Poisson distributions, just as the usual short-range correlation picture does not require a Poisson distribution.[3]

Note that in dominating the x integral of Eq. (4.9) by x near unity, we have implicitly assumed that n is near one of the peaks. Indeed, if n is not sufficiently near any of the peaks, and if $\gamma_0\gamma_1/\alpha'$ is sufficiently large, the x integral will not be dominated by $x = 1$. However, for these n we expect nonleading contributions to F_N and high-mass diffractive dissociation to be important. High-mass diffraction will be discussed in the next section.

Le Bellac[10] has argued that the absence of long-range correlations requires all σ_n/σ to decrease faster than any power of Y at fixed n. A simple application of unitarity then shows that σ also decreases faster than any power of Y, thus ruling out a Pomeron intercept of unity. We now show that the Pomeron cuts introduce long-range correlations sufficient to remove this difficulty. Following Le Bellac,[10] consider the quantities

$$\mu_N = \langle (n - \langle n\rangle)^N\rangle. \tag{4.11}$$

Any μ_N can be expressed as an Nth-order polynomial in the f_n. Le Bellac showed that if all the f_n grow linearly in Y, then μ_{2N} grows at most as Y^N. If $\langle n\rangle$ grows as Y, we than have for small n

$$\frac{\sigma_n}{\sigma} \leq \frac{\mu_{2N}}{(n - \langle n\rangle)^{2N}} = O(Y^{-N}). \tag{4.12}$$

Summing over the diffractive cross section with small n, we obtain

$$\frac{\sigma_{\text{diff}}}{\sigma} = O(Y^{-N}). \tag{4.13}$$

Since N is arbitrary, $\sigma_{\text{diff}}/\sigma$ goes to zero faster than any power of Y.

Suppose now that the f_n behave as in Eq. (4.7). An argument similar to that of Le Bellac then shows that

$$\mu_N = f_n + O(Y^{n-2})$$
$$= \frac{N_0^2 \gamma_0^n Y^{n-1}(2+(-1)^n)}{32\pi\alpha' \beta_0^2} + O(Y^{n-2}). \quad (4.14)$$

Putting this into the above argument, we only find

$$\sigma_{\text{diff}} \lesssim \frac{3N_0^2}{32\pi\alpha' m^2 Y} = O(Y^{-1}), \quad (4.15)$$

as expected in a Regge-pole model. Using Eq. (4.10) we obtain

$$\sigma_{\text{diff}} \lesssim 3\sigma_{\text{diff}}. \quad (4.16)$$

This is a check on the internal consistency of the model. The factor of 3 occurs because the second peak in the multiplicity distribution at $n = 2\gamma_0 Y$ contributes to μ_{2N} twice as much as the diffractive piece.

V. POMERON INTERACTIONS

In previous sections we restricted ourselves to graphs in the Reggeon calculus not involving interactions among Pomerons. In this section we extend our discussion to all graphs with at most a single Pomeron loop. Thus we consider all of the graphs in Figs. 1(b) and 2. As before, our procedure is to study the contributions of various cuttings of these diagrams to the absorptive part of the forward elastic amplitude. For each cutting we isolate n particles from the final state to determine a contribution to the n-particle inclusive reaction.

Pomeron interactions immediately present the problem of renormalization in the Reggeon calculus.[6] In this section we consider all vertices as the unrenormalized quantities. In Sec. II we worked with renormalized vertices and assumed that any extra polynomials in Y occurring in the expression for the total cross section were canceled by appropriate counterterms. Such a procedure could also be used here to calculate the F_n. In using the generating function, however, one loses track of the individual F_n and it is no longer clear which terms correspond to renormalizations. Because of the simplification provided by the generating function, we prefer to use it and therefore to work with unrenormalized quantities. The two procedures are equivalent, and one may at the end rewrite all quantities in terms of renormalized vertices.

We use $\bar{\beta}_0$ to denote the unrenormalized Pomeron-particle-particle coupling at zero momentum transfer. We parametrize $\bar{N}(k_\perp^2)$ and $\gamma(k_\perp^2)$ as in Eqs. (3.3) and (3.16). For the triple-Pomeron coupling we take

$$g(0, k_\perp) = -g_0 k_\perp^2 e^{g_1 k_\perp^2}, \quad (5.1)$$

satisfying Eq. (2.8). The Pomeron intercept will be renormalized, so we set

$$\alpha(t) = 1 + \omega + \alpha' t,$$

where ω is to be determined. In considering one-loop diagrams we drop all terms of higher order in N_0 and g_0 than N_0^2, $N_0 g_0$, and g_0^2. The shift in $\alpha(0)$ from unity occurs only in order g_0^2; thus, in the one-loop approximation only the pole diagram is affected by this shift. In particular we keep the condition that the triple-Pomeron coupling vanishes at $k_\perp^2 = 0$.

To illustrate the renormalization procedure and conventions, we give the expression for the total cross section arising from the diagrams of Figs. 1(b) and 2:

$$m^2\sigma = \bar{\beta}_0^2 e^{\omega Y} - \frac{N_0^2}{4}\int \frac{d^2k_\perp}{(2\pi)^2} e^{2\alpha' k_\perp^2 Y + 2N_1 k_\perp^2} - \frac{2N_0 g_0 \bar{\beta}_0}{4}\int_0^Y d\xi \int \frac{d^2k_\perp}{(2\pi)^2}(-k_\perp^2) e^{2\alpha' k_\perp^2 \xi + N_1 k_\perp^2 + g_1 k_\perp^2}$$
$$- \frac{g_0^2 \bar{\beta}_0^2}{4}\int_0^Y d\xi_1 \int_0^{Y-\xi} d\xi_2 \int \frac{d^2k_\perp}{(2\pi)^2}(-k_\perp^2)^2 e^{2\alpha' k_\perp^2 (Y-\xi_1-\xi_2) + 2g_1 k_\perp^2}. \quad (5.2)$$

The integrations are elementary and give

$$m^2\sigma = \bar{\beta}_0^2 + \bar{\beta}_0^2 \omega Y + O(\omega^2) - \frac{N_0^2}{32\pi(\alpha' Y + N_1)} - \frac{N_0 g_0 \bar{\beta}_0}{16\pi\alpha'}\left(\frac{1}{N_1 + g_1} - \frac{1}{2\alpha' Y + N_1 + g_1}\right) - \frac{g_0^2 \bar{\beta}_0^2}{128\pi\alpha'^2}\left(\frac{\alpha' Y}{g_1^2} - \frac{1}{g_1} + \frac{1}{\alpha' Y + g_1}\right). \quad (5.3)$$

We wish to remove the term proportional to Y in Eq. (5.3) so that the asymptotic cross section will be constant in the one-loop approximation. This requires setting

$$\omega = \frac{g_0^2}{128\pi\alpha' g_1^2}. \quad (5.4)$$

Hence, we obtain

$$m^2\sigma_T = \left(\bar{\beta}_0^2 - \frac{N_0 g_0 \bar{\beta}_0}{16\pi\alpha'(N_1+g_1)} + \frac{g_0^2\bar{\beta}_0^2}{128\pi\alpha'^2 g_1}\right) - \frac{1}{32\pi\alpha' Y}\left(N_0 - \frac{g_0\bar{\beta}_0}{2\alpha'}\right)^2 + O\left(\frac{1}{Y^2}\right). \quad (5.5)$$

Defining the renormalized vertex β_0 by

$$\lim_{Y\to\infty} m^2\sigma = \beta_0^2, \quad (5.6)$$

we find, to the order in which we are working,

$$\beta_0 = \bar{\beta}_0 - \frac{N_0 g_0}{32\pi\alpha'(N_1+g_1)} + \frac{g_0^2\bar{\beta}_0}{256\pi\alpha'^2 g_1}. \quad (5.7)$$

To obtain information on inclusive cross sections, we now cut the diagrams of Figs. 1(b) and 2. We again calculate the generating function from

$$\sigma\psi(\lambda) = \sum_{n=0}^{\infty}\frac{(\lambda-1)^n}{n!}\sigma F_n = \sum_{n=0}^{\infty}\frac{(\lambda-1)^n}{n!}\int dp_1\cdots dp_n\,\frac{d\sigma}{dp_1\cdots dp_n}. \quad (5.8)$$

The differential inclusive cross section from a particular cut diagram is given by an integral similar to those in Eq. (5.1) but with factors of $\gamma(p_\perp, k_\perp)$ inserted for each particle removed from a cut Pomeron. See Figs. 11 and 12. The sum over n in Eq. (5.8) can be replaced with a multiple sum over the number of particles isolated from each cut Pomeron. Each cut Pomeron then contributes to $\psi(\lambda)$ a factor

$$\exp[\xi(\lambda-1)\gamma_0 e^{k_\perp^2\gamma_1}], \quad (5.9)$$

where ξ is the rapidity gap spanned by the cut Pomeron, and $k_\perp^2$ is its transverse momentum. Keeping only one-loop contributions, we write

$$\sigma\psi(\lambda) = \sum_G \sigma\psi(\lambda)\Big|_G, \quad (5.10)$$

where the sum over G denotes a sum over the contributions of the various graphs. We label the graphs by the respective figure numbers. The previous section calculated the contributions of Figs. 8 and 9. From Fig. 11 we obtain

$$m^2\sigma\psi(\lambda)\Big|_{\text{Fig. 11}} = \frac{2N_0 g_0\bar{\beta}_0}{4}\int_0^Y d\xi\int\frac{d^2k_\perp}{(2\pi)^2}(-k_\perp^2)e^{(2\alpha'\xi+N_1+g_1)k_\perp^2}\{\exp[(Y-\xi)(\lambda-1)\gamma_0]\} \times\{2\exp[2\xi(\lambda-1)\gamma_0 e^{k_\perp^2\gamma_1}] - 4\exp[\xi(\lambda-1)\gamma_0 e^{k_\perp^2\gamma_1}] + 1\}. \quad (5.11)$$

Changing integration variables, we rewrite this as

$$m^2\sigma\psi(\lambda)\Big|_{\text{Fig. 11}} = \frac{N_0 g_0\bar{\beta}_0}{8\pi\gamma_1^2}\int_0^1 du\int_0^1\frac{dx}{x}(-Y\ln x)x^{(2\alpha' Yu+N_1+g_1)/\gamma_1} \times\{2\exp[Y(\lambda-1)\gamma_0(1-u+2ux)] - 4\exp[Y(\lambda-1)\gamma_0(1-u+ux)] + \exp[Y(\lambda-1)\gamma_0(1-u)]\}. \quad (5.12)$$

Similarly, the contribution from the graph of Fig. 12 is

$$m^2\sigma\psi(\lambda)\Big|_{\text{Fig. 12}} = \frac{g_0^2\bar{\beta}_0^2}{16\pi\gamma_1^3}\int_0^1 du\int_0^{1-u} dv\int_0^1\frac{dx}{x}(-Y\ln x)^2 x^{(2\alpha' Y(1-u-v)+2g_1)/\gamma_1} \times\{2\exp[Y(\lambda-1)\gamma_0(u+v+2x(1-u-v))] - 4\exp[Y(\lambda-1)\gamma_0(u+v+x(1-u-v))] + \exp[Y(\lambda-1)\gamma_0(u+v)]\}. \quad (5.13)$$

From the generating function we can immediately calculate the f_n. Keeping only the leading order in Y, we obtain for $n \geq 3$

$$f_n = +\frac{\gamma_0^n Y^{n-1}(2+(-1)^n)}{32\pi\alpha'\bar{\beta}_0^2} \times\left[N_0^2 + \frac{N_0 g_0\bar{\beta}_0}{\alpha'(n-1)} + \frac{g_0^2\bar{\beta}_0^2}{2\alpha'^2(n-1)(n-2)}\right] + O(Y^{n-2}). \quad (5.14)$$

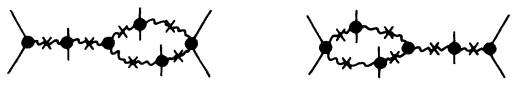

(a) (b)

FIG. 11. The singly enhanced cut graphs for the n-particle inclusive cross section. All possible cuttings and arrangments of the produced particles should be included.

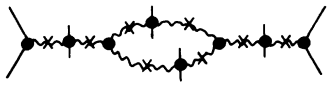

FIG. 12. The doubly enhanced cut graph for the n-particle inclusive cross section. All possible cuttings and arrangements of the produced particles should be included.

The cases $n=1$ and $n=2$ are anomalous. For $n=1$ we find

$$f_1=\langle n\rangle = \left(\gamma_0+\frac{g_0^2\gamma_0}{128\pi\alpha'^2 g_1}\right)Y + \left(\frac{N_0 g_0\gamma_0}{32\pi\alpha'^2\bar\beta_0}-\frac{g_0^2\gamma_0}{64\pi\alpha'^3}\right)\ln Y + O(1). \quad (5.15)$$

The term linear in Y contains a piece which should be interpreted as a renormalization of the vertex γ. For $n=2$ we obtain

$$f_2=\frac{3g_0^2\gamma_0^2 Y\ln(\alpha' Y/g_1)}{64\pi\alpha'^3} + \frac{3\gamma_0^2 Y}{32\pi\alpha'\bar\beta_0^2}\left[N_0^2+\frac{N_0 g_0\bar\beta_0}{\alpha'}-\frac{5g_0^2\bar\beta_0^2}{4\alpha'^2}\right]+O(1). \quad (5.16)$$

Short-range effects will modify the $O(Y)$ term. However, we again remind the reader of the discussion in Sec. II: The cut contribution should behave essentially as Y^2 in the NAL to CERN-ISR energy range. Note that in the limit $Y\to\infty$ the long-range correlation becomes apparent in f_2, although only as a $\ln Y$ effect.

Keeping in mind the cautionary remarks of the last section, we find the multiplicity distribution by differentiation. Again labeling by the respective graphs, we write

$$\sigma_n=\sum_G \sigma_n\Big|_G . \quad (5.17)$$

The graphs of Figs. 8 and 9 were discussed in the last section. Designating a Poisson distribution by

$$P_n(Z)=\frac{Z^n}{n!}e^{-Z}, \quad (5.18)$$

we find

$$m^2\sigma_n|_{\text{Fig. 11}}=\frac{N_0 g_0\bar\beta_0}{8\pi\gamma_1^2}\int_0^1 du\int_0^1\frac{dx}{x}(-Y\ln x)x^{(2\alpha' Yu+N_1+g_1)/\gamma_1} \times[2P_n(\gamma_0 Y(1-u+2ux))-4P_n(\gamma_0 Y(1-u+ux))+P_n(\gamma_0 Y(1-u))], \quad (5.19)$$

and

$$m^2\sigma_n|_{\text{Fig. 12}}=\frac{g_0^2\bar\beta_0^2}{16\pi\gamma_1^3}\int_0^1 du\int_0^{1-u}dv\int_0^1\frac{dx}{x}(-Y\ln x)^2 x^{(2\alpha'-Y(1-u-v)+2g_1)\gamma_1} \times[2P_n(\gamma_0 Y(u+v+2x(1-u-v)))-4P_n(\gamma_0 Y(u+v+x(1-u-v)))+P_n(\gamma_0 Y(u+v))]. \quad (5.20)$$

These expressions are superpositions of Poisson distributions centered between $n=0$ and $n=2\gamma_0 Y$.

We now study in more detail the terms in Eq. (5.19). As in the last section, we dominate the x integrals by x near unity. Then Eq. (5.19) becomes

$$m^2\sigma_n|_{\text{Fig. 11}}\approx\frac{N_0 g_0\bar\beta_0}{32\pi\alpha'^2 Y}\int_0^1\frac{du}{[u+(N_1+g_1)/2\alpha' Y]^2}[2P_n(\gamma_0 Y(1+u))-4P_n(\gamma_0 Y)+P_n(\gamma_0 Y(1-u))]. \quad (5.21)$$

The first of the Poisson distributions under this integral peaks at $n=\gamma_0 Y(1+u)$ and thus tends to fill the gap between $n=\gamma_0 Y$ and $n=2\gamma_0 Y$ in the noninteracting Pomeron prediction. The second term reduces the size of the peak at $n=\gamma_0 Y$. The third term fills in the gap between $n=0$ and $n=\gamma_0 Y$. This third term corresponds to the physical process where one incident particle is diffractively dissociated into a low-mass state while the other is excited into a massive system through the triple-Pomeron coupling, as in Fig. 13. Clearly the cutting which does not cut the loop Pomerons in Fig. 2(d) corresponds to the process of both initial particles being diffractively dissociated into massive states via the triple-Pomeron process. We note that the last term of Eq. (5.21) yields

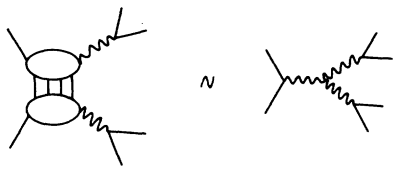

FIG. 13. High-mass diffractive dissociation via the triple-Pomeron vertex.

$$\lim_{Y\to\infty} m^2\sigma_n(Y) = \frac{N_0 g_0 \bar{\beta}_0}{32\pi\alpha'^2\gamma_0 Y^2} + O\left(\frac{1}{Y^3}\right), \qquad (5.22)$$

where n is fixed but large enough that low-multiplicity diffraction is negligible.

ACKNOWLEDGMENTS

We wish to thank Ling-Lie Wang for her collaboration in an earlier, unpublished work on Regge cuts and inclusive reactions. We also wish to thank Chris Hamer and Chung-I Tan for helpful discussions about multi-Regge models.

APPENDIX

Since the $k_\perp$ dependence of the central vertex $\gamma(p_\perp, k_\perp)$ is not directly measurable, it must be estimated from a model. The simplest reasonable model is a straightforward generalization to nonzero $k_\perp$ of the one considered by Silverman and Tan.[23] It is motivated by the multi-Regge idea[24-30]: The exchange of an internal Reggeon with a trajectory $\alpha_R(t)$ builds up the Pomeron with a trajectory $\alpha(t)$. The vertex $\gamma(p_\perp, k_\perp)$ is therefore to be extracted from the graph for the non-forward six-point function shown in Fig. 14. The appropriate discontinuity[1,16] of the amplitude is

$$\begin{aligned}\mathrm{disc}F(s,k,p) = 2i\int \frac{d^4q}{(2\pi)^4}&[\beta(t) g_{RRP}(t, t_l^+, t_l^-)(s_l'/m^2)^{\alpha(t)}]\\ &\times (s_l/s_l')^{\alpha_R(t_l^+)+\alpha_R(t_l^-)}\Gamma_{RR}(t_l^+, t_r^+)\Gamma_{RR}(t_l^-, t_r^-)(s_r/s_r')^{\alpha_R(t_r^+)+\alpha_R(t_r^-)}\\ &\times[\beta(t) g_{RRP}(t, t_r^+, t_r^-)(s_r'/m^2)^{\alpha(t)}],\end{aligned} \qquad (A1)$$

where

$$\begin{aligned} s &= (p_a+p_b)^2, & t &= k^2,\\ u_l &= (p_a-p)^2, & u_r &= (p_b-p)^2,\\ s_l' &= (p_a+\tfrac{1}{2}k-\tfrac{1}{2}p-q)^2, & s_r' &= (p_b-\tfrac{1}{2}k-\tfrac{1}{2}p+q)^2,\\ s_r &= (p_a+\tfrac{1}{2}k+\tfrac{1}{2}p-q)^2, & s_r &= (p_b-\tfrac{1}{2}k+\tfrac{1}{2}p+q)^2,\\ t_l^+ &= (\tfrac{1}{2}k+\tfrac{1}{2}p+q)^2, & t_r^+ &= (-\tfrac{1}{2}k+\tfrac{1}{2}p-q)^2,\\ t_l^- &= (\tfrac{1}{2}k-\tfrac{1}{2}p-q)^2, & t_r^- &= (-\tfrac{1}{2}k-\tfrac{1}{2}p+q)^2, \end{aligned} \qquad (A2)$$

and the vertex functions are defined in the obvious way.

In principle one could determine all the trajectory and vertex functions in Eq. (A1) by solving some multi-Regge equation.[28-30] It is known, however, that it is not possible to make a simple multi-Regge equation give results consistent with experiment.[31] It is therefore better to adopt the approach of Silverman and Tan and to assume reasonable forms for these quantities. The trajectories are taken to be linear:

$$\begin{aligned}\alpha(t) &= \alpha_0 + \alpha' t\\ \alpha_R(t) &= \alpha_{0R} + \alpha_R' t.\end{aligned} \qquad (A3)$$

The vertex functions are taken to be exponentials:

$$\begin{aligned}\beta(t) &= \beta_0 e^{\beta_1 t},\\ g_{RRP}(t, t_1, t_2) &= G_0 e^{a_1(t_1+t_2)} e^{\beta_1 t},\\ \Gamma_{RR}(t_1, t_2) &= \Gamma_0 e^{a_2(t_1+t_2)}.\end{aligned} \qquad (A4)$$

Note that the t dependence of g_{RRP} has been taken to be the same as that of β, since presumably $g_{RRP}(t, m^2, m^2) = \beta(t)$. However, the values of a_1, a_2, and β_1 are not assumed to be related.

To simplify the calculation it is helpful to make the usual multi-Regge kinematic approximations. These are that the momentum transfers are transverse, and that

$$\begin{aligned} &s_l' \le -u_l, \quad s_r' \le -u_l,\\ &s_l \approx -u_l, \quad s_r \approx -u_r,\\ &d^4q \approx \frac{1}{2s} ds_l' ds_r' d^2q_\perp. \end{aligned} \qquad (A5)$$

Letting

$$s_l' = -x_l u_l, \quad s_r' = -x_r u_r, \qquad (A6)$$

one then readily finds

$$\mathrm{disc}F = \frac{1}{s}(u_l u_r)^{\alpha(k_\perp^2)+1}\beta^2(k_\perp^2)\gamma(p_\perp, k_\perp),$$

where

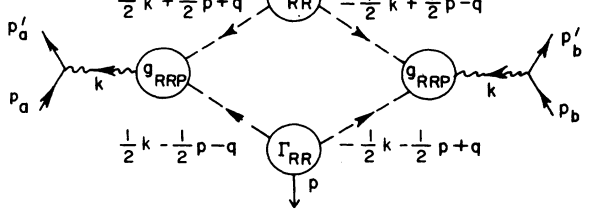

FIG. 14. The graph for a model of the vertex $\gamma(p_\perp, k_\perp)$.

$$\gamma(p_\perp, k_\perp) = \text{const} \times e^{2\beta_1 k_\perp^2} e^{(a_1+a_2)(p_\perp^2+k_\perp^2)} \times \int_0^1 dx_l dx_r \int d^2q_\perp e^{4(a_1+a_2)q_\perp^2} (x_l)^{\alpha(k_\perp^2)-2\alpha_R(k_\perp^2/4)} (x_r)^{\alpha(k_\perp^2)-2\alpha_R(k_\perp^2/4)-\alpha_R' p_\perp/2-q_\perp)^2}. \quad \text{(A7)}$$

The x_l and x_r integrals are trivial. The remaining $q_\perp$ integral can be simplified by ignoring the $q_\perp$ dependence everywhere except in the exponential, as will be justified *a posteriori*. Then

$$\gamma(p_\perp, k_\perp) = \text{const} \times e^{2\beta_1 k_\perp^2} e^{(a_1+a_2)(p_\perp^2+k_\perp^2)} [2(1-\alpha_R) + \alpha' k_\perp^2 - \tfrac{1}{2}\alpha_R'(p_\perp^2+k_\perp^2)]^{-2}$$
$$\approx \text{const} \times \exp\left\{2\left[\beta_1 - \frac{\alpha'}{2(1-\alpha_{0R})}\right]k_\perp^2 + \left[a_1+a_2+\frac{\alpha_R'}{2(1-\alpha_{0R})}\right](p_\perp^2+k_\perp^2)\right\}, \quad \text{(A8)}$$

where all of the $p_\perp^2$ and $k_\perp^2$ dependence has been approximated by exponentials. With $\alpha_{0R} = \frac{1}{2}$ and $a = a_1 + a_2 + \alpha_R'$ this formula gives Eq. (3.16). Because of the small value of $\langle p_\perp^2 \rangle$, it also shows that dropping the $q_\perp$ dependence in Eq. (A7) everywhere except in the exponential was justified.

It should perhaps be noted that if one actually solves the multi-Regge integral equation with a kernel

$$K(t_l^+, t_l^-; t_r^+, t_r^-) = \Gamma_0^2 e^{\bar{a}(t_l^+ + t_l^- + t_r^+ + t_r^-)}, \quad \text{(A9)}$$

a form suggested by the above choice of Γ_{RR}, one finds that the $k_\perp$ falloff of $\gamma(p_\perp, k_\perp)$ is slower than the $p_\perp$ falloff. This occurs because the value of α' obtained is very large, so that the quantity $[\beta_1 - \alpha'/2(1-\alpha_{0R})]$ in Eq. (A8) is negative. The experimental value of α' is of course small.

*Work performed under the auspices of the U. S. Atomic Energy Commission.

[1] A. H. Mueller, Phys. Rev. D 2, 2963 (1970).
[2] K. Wilson, Cornell Univ. Report No. CLNS 131, 1970 (unpublished).
[3] A. H. Mueller, Phys. Rev. D 4, 150 (1971).
[4] V. A. Abramovskii, O. V. Kanchelli, and V. N. Gribov, in *Proceedings of the XVI International Conference on High Energy Physics, Chicago-Batavia, Ill., 1972,* edited by J. D. Jackson and A. Roberts (NAL, Batavia, Ill., 1973), Vol. 1, p. 389.
[5] V. N. Gribov, Zh. Eksp. Teor. Fiz. 53, 654 (1967) [Sov. Phys.—JETP 26, 414 (1968)].
[6] V. N. Gribov and A. A. Migdal, Yad. Fiz. 8, 1002 (1968) [Sov. J. Nucl. Phys. 8, 583 (1969)]; Yad. Fiz. 1128 (1968) [Sov. J. Nucl. Phys. 8, 703 (1969)].
[7] F. E. Paige and L.-L. Wang, Nucl. Phys. B46, 477 (1972); F. Sannes *et al.*, Phys. Rev. Lett. 30, 766 (1973) and private communication.
[8] T. Ferbel, Phys. Rev. D 7, 925 (1973).
[9] J. C. Botke, Phys. Rev. Lett. 31, 658 (1973).
[10] M. Le Bellac, Phys. Lett. 37B, 413 (1971).
[11] K. A. Ter-Martirosyan, Phys. Lett. 44B, 377 (1973).
[12] H. D. I. Abarbanel, G. F. Chew, M. L. Goldberger, and L. M. Saunders, Phys. Rev. Lett. 26, 937 (1971).
[13] C. E. Jones, F. E. Low, S.-H. H. Tye, G. Veneziano, and J. E. Young, Phys. Rev. D 4, 906 (1971).
[14] R. C. Brower and J. H. Weis, Phys. Lett. 41B, 631 (1972).
[15] I. J. Muzinich, F. E. Paige, T. L. Trueman, and L.-L. Wang, Phys. Rev. Lett. 28, 850 (1972); Phys. Rev. D 4, 1048 (1972).
[16] C.-I Tan, Phys. Rev. D 4, 2412 (1971); H. P. Stapp, *ibid.* 3, 3177 (1971).
[17] A. B. Kaidalov, Yad. Fiz. 13, 401 (1971) [Sov. J. Nucl. Phys. 13, 226 (1971)].
[18] V. Bartenev *et al.*, Phys. Rev. Lett. 29, 1755 (1972).
[19] A. Neuhofer *et al.*, Phys. Lett. 37B, 438 (1971); R. S. Panvini *et al.*, *ibid.* 38B, 55 (1972); British-Scandinavian Collaboration, *ibid.* 44B, 521 (1973); Saclay-Strasbourg Collaboration, *ibid.* 44B, 537 (1973).
[20] Z. Koba, H. Nielsen, and P. Olesen, Nucl. Phys. B40, 317 (1972).
[21] S.-S. Shei and T.-M. Yan, Phys. Rev. D 6, 1744 (1972).
[22] L. S. Brown, Phys. Rev. D 5, 748 (1972).
[23] D. Silverman and C.-I Tan, Nuovo Cimento 2, 489 (1971); Phys. Rev. D 3, 991 (1971).
[24] L. Bertocchi, S. Fubini, and M. Tonin, Nuovo Cimento, 25, 626 (1962); D. Amati, A. Stanghellini and S. Fubini, *ibid.* 26, 896 (1962).
[25] G. F. Chew and A. Pignotti, Phys. Rev. 176, 2112 (1968).
[26] I. G. Halliday and L. M. Saunders, Nuovo Cimento 60A, 115 (1969).
[27] L. Caneschi and A. Pignotti, Phys. Rev. Lett. 22, 1219 (1969).
[28] K. Kajantie, Phys. Rev. 172, 1470 (1968).
[29] G. F. Chew, M. L. Goldberger, and F. E. Low, Phys. Rev. Lett. 22, 208 (1969).
[30] G. F. Chew and W. R. Frazer, Phys. Rev. 181, 1914 (1969).
[31] C. J. Hamer and R. F. Peierls, Phys. Rev. D 8, 1358 (1973); R. C. Hwa, *ibid.* 8, 1331 (1973).